Journal of Liquid Chromatography and Gas Chromatography, Europe
https://technicalreport.org/lcgceu/

LC GC Eu., Vol. 38, No.1, 09-16, 2025

Technical Reports Press

RESEARCH ARTICLE

Spectral-Leverage Separation of Mass-18 Methane Clumped Isotopologues in Mid-Infrared Absorption Calibration

Walter Giger[1*] **and F. Robert**[1]

[1]*Giger Research Consulting, 8049 Zürich, Switzerland*
[*]*Corresponding author*

Corresponding author:
waltergig@swissonline.ch

Received: 28 Augsut 2024
Accepted: 15 December 2024
Available online: 30 March 2025

Abstract

Reliable interpretation of methane $\Delta^{13}CH_3D$ and $\Delta^{12}CH_2D_2$ requires the two mass-18 coordinates to be evaluated together with the absorption-window conditions that generate them. The research question addressed here is whether five measured mid-infrared transitions and twelve EP-reference gas entries can separate high-clump, low-clump, thermally heated, and hydrogen-rich methane states without reducing the classification to a single clumped coordinate. The transition records comprise $^{12}CH_3D$, $^{12}CH_2D_2$, $^{13}CH_3D$, $^{12}CH_4$, and $^{13}CH_4$ lines, while the gas records comprise EP1, EP4, EP6, EP7, and EP6 heated at 300 °C. The analysis calculates the local line-strength share of each target transition, consolidates reported gas coordinates with uncertainty weighting, and compares the resulting positions in paired $\Delta^{13}CH_3D$–$\Delta^{12}CH_2D_2$ space. The $^{12}CH_2D_2$ line contributes 1.10% of the laser-1 line-strength total, whereas the $^{13}CH_3D$ line contributes 11.29% of the laser-2 total. This spectral imbalance explains why $\Delta^{12}CH_2D_2$ is a powerful but line-limited coordinate, while $\Delta^{13}CH_3D$ has greater direct leverage but remains affected by neighboring methane absorptions. The calibrated gas positions separate EP6 and EP1 as high-clump references, EP7 as a lower-clump displaced gas, EP6-HG300 as a heated low-clump gas, and EP4 as a hydrogen-rich gas with $\Delta^{12}CH_2D_2$ of 17.34‰. The main finding is that mid-infrared methane clumped-isotope calibration must preserve both mass-18 coordinates and report the local absorption-window structure supporting each coordinate.

Keywords: methane clumped isotopes; analytical spectroscopy; mid-infrared absorption; reference-gas calibration; isotopologue selectivity; $\Delta^{13}CH_3D$; $\Delta^{12}CH_2D_2$; absorption-window leverage

1. Introduction

Methane isotope analysis is central to analytical chemistry, environmental geochemistry, energy-resource characterization, and atmospheric source attribution. Bulk $\delta^{13}C$–CH_4 and δD–CH_4 values record substrate origin, methanogenic pathway, thermal maturity, mixing, oxidation, and migration history. These two bulk coordinates, however, may overlap among microbial, thermogenic, abiotic, and altered methane systems after transport or secondary reaction. Carbon-hydrogen isotope diagrams therefore identify broad domains of methane origin but do not always reveal whether a gas preserves its formation state or has undergone thermal reordering, hydrogen exchange, microbial overprinting, or physical mixing [1–4].

Clumped-isotope analysis adds molecular-ordering information by measuring departures from stochastic rare-isotope distribution within methane molecules. Early carbonate applications established the analytical value of multiply substituted isotopologues before comparable concepts were applied to methane [5]. The two mass-18 methane isotopologues, $^{13}CH_3D$ and $^{12}CH_2D_2$, carry information that cannot be reconstructed from bulk $\delta^{13}C$–CH_4 and δD–CH_4 alone. Equilibrium theory predicts decreasing rare-isotope ordering with increasing temperature, whereas non-equilibrium departures can arise from kinetic isotope effects, enzymatic reversibility, anaerobic oxidation, mixing between isotope reservoirs, and post-generation alteration [6–8].

Cite as: W. Giger & F. Robert (2025). Spectral-Leverage Separation of Mass-18 Methane Clumped Isotopologues in Mid-Infrared Absorption Calibration. LC GC Eu., 38(1) (2025) 09-16.

Methane clumped isotopologues can therefore act as temperature-sensitive molecular coordinates in appropriate systems and as indicators of non-equilibrium reaction history where simple thermometry would be misleading.

The measurement is analytically demanding because both target isotopologues occur at very low abundance relative to the principal methane isotopologues. High-resolution isotope-ratio mass spectrometry has advanced paired measurement of $^{13}CH_3D$ and $^{12}CH_2D_2$, while tunable mid-infrared laser absorption provides a direct molecular route for interrogating selected transitions with high specificity [9–12]. Laser absorption can use intense fundamental vibrational bands and compact optical cells, but it requires careful line selection, pressure control, gas purification, absorption-continuum stability, and reference-gas transfer. The final isotope coordinate is therefore inseparable from the local spectral environment used to retrieve it.

Laser-spectroscopic applications now target windows around $^{12}CH_2D_2$ and $^{13}CH_3D$ transitions with high-sensitivity gas handling and calibration strategies [13, 14]. This analytical setting raises a specific question: if $\Delta^{13}CH_3D$ and $\Delta^{12}CH_2D_2$ are retrieved from different absorption windows, and if the target transitions occupy different shares of their local line-strength totals, can both coordinates be interpreted with equivalent confidence? The answer matters because a dual-clump reference space can separate heated methane from hydrogen-rich or kinetically altered methane only when each coordinate is judged against its own spectral leverage.

Paired-coordinate interpretation is increasingly required in methane clumped-isotope research. Microbial methane can display non-equilibrium clumped signatures linked to reaction rate and hydrogen availability; anaerobic oxidation can move samples through $\Delta^{13}CH_3D$–$\Delta^{12}CH_2D_2$ space along trajectories that do not match simple equilibrium cooling; and natural-gas accumulations can contain apparent abiotic or thermogenic signatures that require several isotope coordinates for discrimination [15–19]. Large compilations also show that methane clumped-isotope applications are limited by comparability among laboratories, instruments, and sample categories [20]. These observations justify a measurement-level treatment in which spectral selectivity, reference gases, and paired molecular interpretation are analyzed together.

The research question is whether a leverage-normalized reference space built from measured absorption-line strengths and interlaboratory EP-gas values can distinguish high-clump, low-clump, heated, and hydrogen-rich methane states without collapsing the result to one clumped coordinate. The calibration record is deliberately defined by five transition entries and twelve isotope entries: $^{12}CH_3D$, $^{12}CH_2D_2$, $^{13}CH_3D$, $^{12}CH_4$, and $^{13}CH_4$ lines; and $\delta^{13}C$–CH_4, δD–CH_4, $\Delta^{13}CH_3D$, and $\Delta^{12}CH_2D_2$ values for EP1, EP4, EP6, EP7, and EP6-HG300. The scope is analytical spectroscopy rather than methane provenance alone; the classification depends on absorption-window leverage, reference-gas coverage, and paired mass-18 coordinates.

The analytical sequence in Figure 1 connects molecular targets to gas classification. The diagram prevents the final coordinate plot from being read as a stand-alone geochemical diagram. Each interpretation begins with the selected absorption lines, continues through reference-gas coverage and coordinate consolidation, and ends with the paired $\Delta^{13}CH_3D$–$\Delta^{12}CH_2D_2$ separation.

The sequence shown in Figure 1 establishes the order of inference used throughout the article. Methane isotopologues are first treated as spectroscopic targets with different line strengths and neighboring absorptions. Reference gases then supply the calibration coordinates, and the final paired-coordinate space tests whether those coordinates retain chemically meaningful separation.

2. Materials and methods

2.1. Calibration records and analytical boundaries

Five spectroscopic entries and twelve reference-gas isotope entries define the calculation. The spectroscopic entries are line position, line strength, lower-state energy where available, and pressure-broadening information for $^{12}CH_3D$, $^{12}CH_2D_2$, $^{13}CH_3D$, $^{12}CH_4$, and $^{13}CH_4$. The isotope entries are the reported $\delta^{13}C$–CH_4, δD–CH_4, $\Delta^{13}CH_3D$, and $\Delta^{12}CH_2D_2$ values for EP6, EP1, EP7, EP6-HG300, and EP4 measured by Empa, Tokyo Tech, and Utrecht University where available [14]. The calibration record is intentionally compact: it contains reference gases with known contrasts rather than a broad inventory of natural methane samples.

Three calculations were performed. First, each selected transition was expressed as a percentage of total line strength within its own laser group, giving a direct estimate of local spectroscopic leverage. Second, clumped-isotope coordinates reported by more than one laboratory were consolidated with greater weight assigned to lower reported uncertainty; gases reported by a single laboratory were retained as single measured coordinates. Third, EP-gas positions were interpreted in paired $\Delta^{13}CH_3D$–$\Delta^{12}CH_2D_2$ space relative to EP6, allowing heated contraction, low-clump displacement, and hydrogen-rich enrichment to be distinguished from one another.

2.2. Spectroscopic line set

The selected methane transitions are listed in Table 1. Line-by-line interpretation depends on reliable transition parameters and database-style documentation, as emphasized by successive HITRAN releases [21, 22]. Laser group 1 contains a dominant $^{12}CH_3D$ transition and a much weaker $^{12}CH_2D_2$ transition. Laser group 2 contains the $^{13}CH_3D$ transition for the carbon-deuterium clumped coordinate, together with stronger $^{12}CH_4$ and $^{13}CH_4$ lines. Missing lower-state energy and broadening entries for $^{12}CH_2D_2$ are not estimated; their absence is treated as part of the analytical constraint on that weak transition.

The values in Table 1 define a strongly unequal measurement setting. In laser group 1, the $^{12}CH_2D_2$ line is nearly two orders of magnitude weaker than the neighboring $^{12}CH_3D$ line. In laser group 2, $^{13}CH_3D$ is more accessible but is still measured inside a window dominated by major methane isotopologues. Sensitivity is therefore not determined by isotopologue identity alone; it depends on the local absorption neighborhood of each target.

The absorption windows in Figure 2 show the same line hierarchy graphically. The paired presentation makes clear that the two clumped coordinates enter the calibration from different instrumental conditions.

The side-by-side comparison in Figure 2 shows a weak $^{12}CH_2D_2$ measurement beside a dominant $^{12}CH_3D$ feature in laser group 1, and a stronger but still subordinate $^{13}CH_3D$ measurement beside two major methane absorptions in laser group 2. This contrast supports coordinate-specific confidence treatment rather than a single uncertainty assumption for both clumped axes.

A closer view of the first window appears in Figure 3. The separated panel makes the low leverage of the doubly deuterated methane transition explicit.

The analytical implication of Figure 3 is that $^{12}CH_2D_2$ should be treated as a high-value but line-limited signal. Because the surrounding intensity scale is set by $^{12}CH_3D$, small residuals, pressure-dependent line-shape mismatch, or continuum-placement error can disproportionately affect the recovered $\Delta^{12}CH_2D_2$ coordinate.

The second window is isolated in Figure 4. The panel shows that $^{13}CH_3D$ is more visible than $^{12}CH_2D_2$ but still not the dominant absorption in its window.

The second-window view in Figure 4 indicates a different retrieval chal-

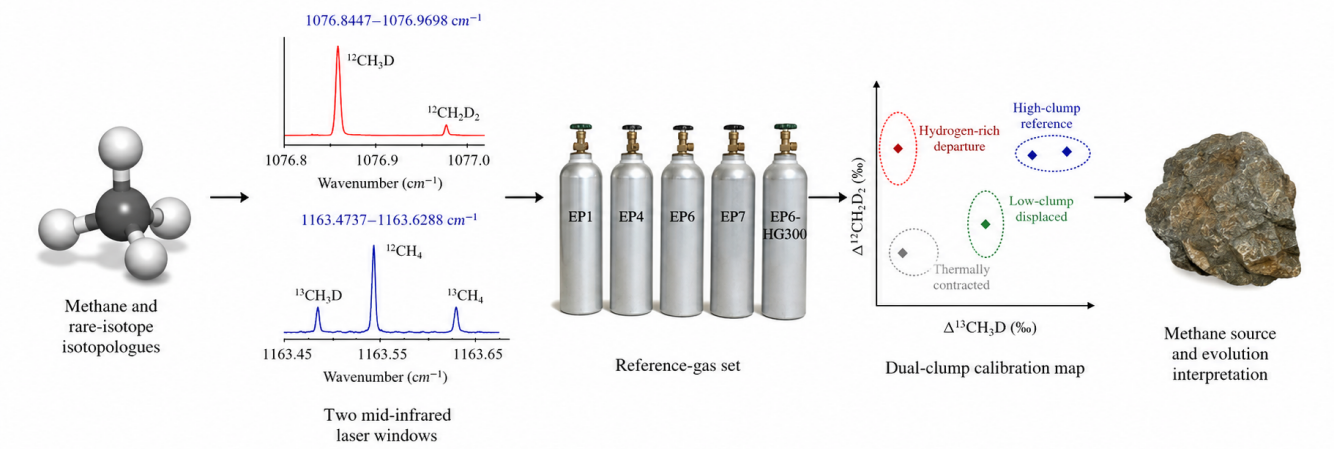

Figure 1: Spectral calibration sequence.

Table 1: Selected line parameters.

Laser group	Species	Position (cm^{-1})	Line strength (cm $molecule^{-1}$)	Additional parameters
Laser 1	$^{12}CH_3D$	1076.8447	1.416×10^{-25}	Lower-state energy 313.1903; broadening 0.080
Laser 1	$^{12}CH_2D_2$	1076.9698	1.575×10^{-27}	Not tabulated
Laser 2	$^{13}CH_3D$	1163.4737	5.940×10^{-26}	Lower-state energy 7.7536; broadening 0.086
Laser 2	$^{12}CH_4$	1163.4937	3.270×10^{-25}	Lower-state energy 2055.9170; broadening 0.068
Laser 2	$^{13}CH_4$	1163.6288	1.395×10^{-25}	Lower-state energy 950.1988; broadening 0.067

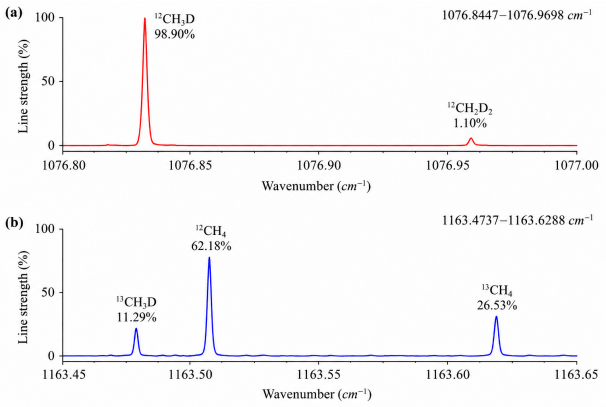

Figure 2: Selected absorption windows.

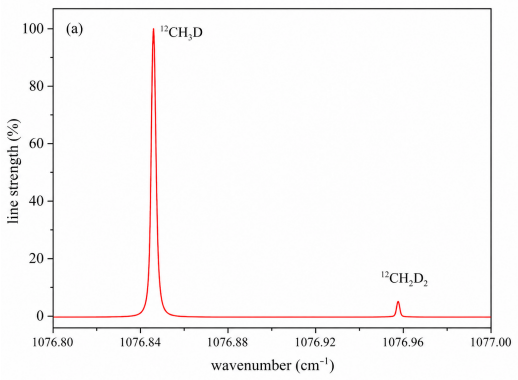

Figure 3: Laser 1 line environment.

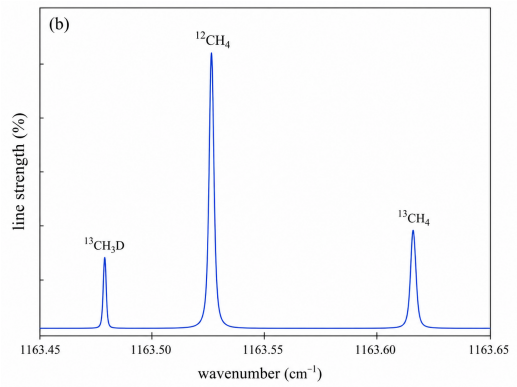

Figure 4: Laser 2 line environment.

lenge. The $^{13}CH_3D$ feature has stronger direct leverage than $^{12}CH_2D_2$, yet its recovery still depends on accurate modeling of adjacent $^{12}CH_4$ and $^{13}CH_4$ absorptions. The $\Delta^{13}CH_3D$ coordinate is therefore less line-limited than $\Delta^{12}CH_2D_2$ but remains sensitive to local spectral fitting.

2.3. Reference-gas isotope records

The EP-gas isotope values are listed in Table 2. EP6, EP1, and EP7 have measurements from three laboratories, EP6-HG300 has measurements from two laboratories, and EP4 has one reported laboratory value. This uneven coverage is part of the calibration evidence. Multi-laboratory gases reveal transferability and spread, whereas EP4 supplies a distinctive hydrogen-rich endpoint because of its unusual δD–CH_4 and $\Delta^{12}CH_2D_2$ pairing.

The entries in Table 2 contain the contrasts required for classification. EP6 and EP6-HG300 have nearly identical Empa $\delta^{13}C$–CH_4 values, -43.75‰ and -43.76‰, but sharply different clumped coordinates. EP4 has $\Delta^{13}CH_3D$ of 1.58‰, close to heated EP6, yet it also has

Table 2: Reference-gas isotope values.

Gas	Laboratory	Replicates	δ^{13}C–CH$_4$	Error	δD–CH$_4$	Error	$\Delta^{13}CH_3D$	Error	$\Delta^{12}CH_2D_2$
EP6	Empa	36	-43.75	–	-188.72	–	3.58	0.02	8.90
EP6	Tokyo Tech	3	-44.15	0.02	-196.56	0.08	3.65	0.10	7.19
EP6	Utrecht	1	-44.35	0.01	-185.80	0.16	3.11	0.33	7.28
EP1	Empa	20	-45.27	0.01	-203.89	0.01	4.10	0.01	8.63
EP1	Tokyo Tech	3	-45.66	0.02	-211.30	0.01	3.92	0.13	9.43
EP1	Utrecht	1	-45.81	0.01	-201.30	0.05	3.94	0.25	9.15
EP7	Empa	20	-37.40	0.01	-163.24	0.01	2.55	0.01	3.76
EP7	Tokyo Tech	3	-37.69	0.01	-171.44	0.03	2.31	0.11	3.38
EP7	Utrecht	1	-37.91	0.01	-160.70	0.10	2.78	0.25	3.09
EP6-HG300	Empa	7	-43.76	0.07	-188.51	0.12	1.66	0.05	3.30
EP6-HG300	Tokyo Tech	3	-44.02	0.21	-196.35	0.22	1.63	0.12	2.96
EP4	Empa	3	-46.21	0.00	-39.93	0.02	1.58	0.01	17.34

δD–CH$_4$ of -39.93 ‰ and $\Delta^{12}CH_2D_2$ of 17.34 ‰. EP7 differs from EP6 in both bulk and clumped coordinates. These specific contrasts allow the paired coordinate system to be tested against false grouping.

The laboratory-coverage structure is summarized in Figure 5. The layout identifies which gases support interlaboratory comparison and which gases serve as distinctive endpoint checks.

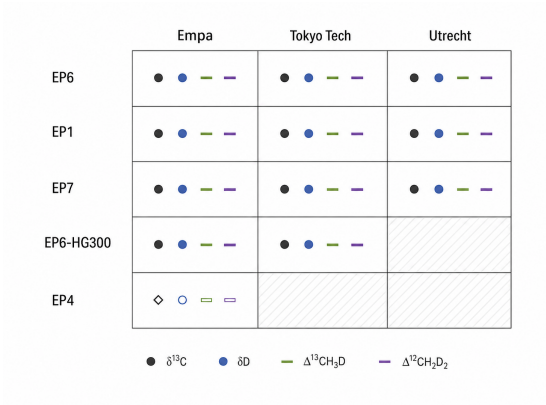

Figure 5: Reference-gas coverage.

The coverage pattern in Figure 5 defines the limits of consolidation. EP6, EP1, and EP7 can be evaluated for interlaboratory spread; EP6-HG300 tests the heating response across two laboratories; and EP4 cannot test transferability by itself but provides a necessary hydrogen-rich contrast because of its unusual δD–CH$_4$–$\Delta^{12}CH_2D_2$ combination.

2.4. Coordinate consolidation and gas-class assignment

Reference-gas coordinates were consolidated by giving greater influence to values with smaller tabulated uncertainty. This operation preserves laboratory spread in the figures while producing one representative coordinate for each gas. Gas-class assignment then used paired behavior. A high-clump reference gas occupies the upper part of both clumped coordinates. A heated gas decreases in both coordinates while retaining close bulk-carbon similarity to its unheated reference. A low-clump displaced gas decreases in both coordinates and also differs in bulk composition. A hydrogen-rich departure displays disproportionate $\Delta^{12}CH_2D_2$ enrichment relative to $\Delta^{13}CH_3D$ and δD–CH$_4$.

This assignment rule is conservative. It does not infer heating from $\Delta^{13}CH_3D$ alone, and it does not treat a high $\Delta^{12}CH_2D_2$ value as sufficient without considering the weak $^{12}CH_2D_2$ line. Classification is accepted only when spectral leverage, laboratory coverage, and paired-coordinate position support the same gas class.

3. Results and discussion

3.1. Absorption-window leverage and coordinate confidence

The local line-strength shares are summarized in Table 3. The $^{12}CH_2D_2$ feature contributes 1.10% of laser group 1, while $^{12}CH_3D$ accounts for 98.90%. In laser group 2, $^{13}CH_3D$ contributes 11.29%, compared with 62.18% for $^{12}CH_4$ and 26.53% for $^{13}CH_4$. These values demonstrate that the two clumped coordinates are not obtained under equivalent spectral leverage.

Table 3: Line-strength shares.

Laser group	Species	Share of group line strength	Analytical interpretation
Laser 1	$^{12}CH_3D$	98.90%	Dominant neighboring absorption feature
Laser 1	$^{12}CH_2D_2$	1.10%	Weak clumped-isotopologue feature with high uncertainty sensitivity
Laser 2	$^{13}CH_3D$	11.29%	Measurable clumped-isotopologue feature
Laser 2	$^{12}CH_4$	62.18%	Dominant major-isotopologue feature
Laser 2	$^{13}CH_4$	26.53%	Secondary major-isotopologue feature

The dominance values in Table 3 explain why $\Delta^{13}CH_3D$ and $\Delta^{12}CH_2D_2$ cannot be assigned identical confidence from the coordinate plot alone. The $^{12}CH_2D_2$ coordinate requires caution for small gas-to-gas differences, while large $\Delta^{12}CH_2D_2$ separations remain diagnostic when they agree with bulk-isotope behavior and the paired $\Delta^{13}CH_3D$ coordinate.

The focused laser-1 view in Figure 6 places the weak $^{12}CH_2D_2$ feature on the same intensity scale as the dominant neighboring line.

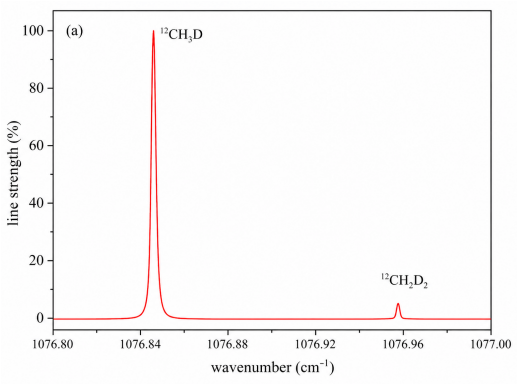

Figure 6: Laser 1 focus.

The practical implication of Figure 6 is that $^{12}CH_2D_2$ retrieval requires careful residual inspection. Its line strength is small enough that apparent $\Delta^{12}CH_2D_2$ changes should be evaluated with reference-gas performance, pressure stability, and agreement with $\Delta^{13}CH_3D$. Under this condition, $\Delta^{12}CH_2D_2$ remains a sensitive discriminant rather than a simple high-precision axis.

The focused laser-2 view in Figure 7 shows a different retrieval problem. The $^{13}CH_3D$ line has a larger share of its window but remains smaller than the principal methane features.

The interpretation of Figure 7 is that $\Delta^{13}CH_3D$ is not independent of spectral context. The target feature is visible, but accurate recovery still depends on modeling stronger neighboring absorptions. A reliable $\Delta^{13}CH_3D$ value therefore requires target-line detection and control of the surrounding absorption field, especially when calibration is transferred across instruments.

The coordinate-leverage contrast is summarized in Figure 8. The panel condenses the line-strength contrast into an instrument-facing comparison between the two clumped coordinates.

The contrast shown in Figure 8 explains why a uniform uncertainty rule is unsuitable. The $^{12}CH_2D_2$ coordinate has strong interpretive value, especially for identifying EP4, but it is retrieved from the line-limited

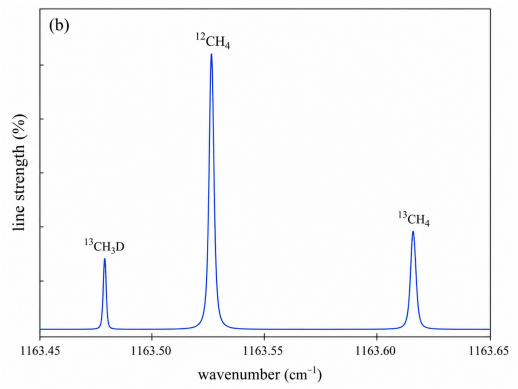

Figure 7: Laser 2 focus.

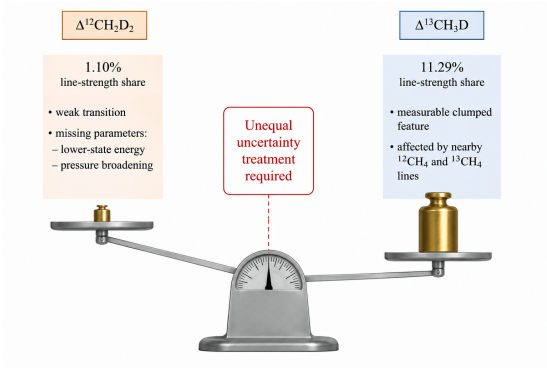

Figure 8: Coordinate leverage contrast.

side of the comparison. The $^{13}CH_3D$ coordinate has stronger line leverage while remaining embedded in a crowded methane window. The two axes complement each other only when this measurement asymmetry is retained.

3.2. Reference-gas consolidation and laboratory spread

The representative clumped coordinates are given in Table 4. EP6 and EP1 define the high-clump reference positions, with EP6 at 3.58 ‰ for $\Delta^{13}CH_3D$ and 8.83 ‰ for $\Delta^{12}CH_2D_2$, and EP1 at 4.10 ‰ and 8.67 ‰, respectively. EP7 is lower in both coordinates, whereas EP6-HG300 and EP4 share similarly low $\Delta^{13}CH_3D$ values but diverge sharply in $\Delta^{12}CH_2D_2$.

Table 4: Consolidated clumped coordinates.

Gas	Representative $\Delta^{13}CH_3D$	Error	Representative $\Delta^{12}CH_2D_2$	Error
EP6	3.58	0.02	8.83	0.22
EP1	4.10	0.01	8.67	0.18
EP7	2.55	0.01	3.76	0.07
EP6-HG300	1.66	0.05	3.20	0.44
EP4	1.58	0.01	17.34	0.20

The values in Table 4 show why one clumped coordinate is insufficient. EP6-HG300 and EP4 are nearly indistinguishable by representative $\Delta^{13}CH_3D$ alone, with values of 1.66 ‰ and 1.58 ‰. Their $\Delta^{12}CH_2D_2$ values differ by more than 14 ‰, a separation far larger than the caution introduced by the weak $^{12}CH_2D_2$ line and therefore large enough to define a distinct gas class.

The distribution of laboratory and representative values is plotted in Figure 9. This comparison separates the reported laboratory entries from the consolidated gas coordinates.

The graphical comparison in Figure 9 shows why the representative positions should not be read as unqualified averages. Laboratory spread is visible for EP6, EP1, and EP7, yet each gas retains a usable

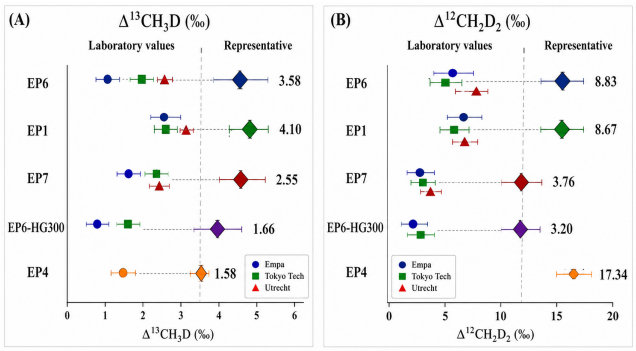

Figure 9: Laboratory and gas coordinates.

calibration position. EP4 remains a single-laboratory point, but its $\Delta^{12}CH_2D_2$ enrichment lies far outside the main reference-gas field, so its role does not depend on small interlaboratory offsets.

3.3. Thermal contraction and hydrogen-rich separation

The EP6 to EP6-HG300 comparison directly tests the heated-gas class. The Empa $\delta^{13}C$–CH_4 values are nearly unchanged, moving only from -43.75 ‰ to -43.76 ‰, whereas representative $\Delta^{13}CH_3D$ decreases from 3.58 ‰ to 1.66 ‰ and representative $\Delta^{12}CH_2D_2$ decreases from 8.83 ‰ to 3.20 ‰. This pattern is a paired-clump contraction without a corresponding bulk-carbon shift.

The contraction comparison is shown in Figure 10. It places bulk carbon and the two clumped coordinates on a common interpretive scale.

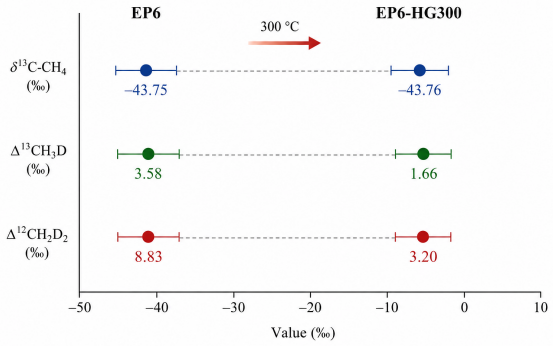

Figure 10: EP6 heating response.

The key result from Figure 10 is that heating changes molecular ordering more clearly than bulk carbon composition. The shift is nearly invisible in $\delta^{13}C$–CH_4 but large in both rare-isotope ordering coordinates. EP6-HG300 therefore gives an internal check that the paired clumped coordinates can detect thermal contraction without requiring a bulk-carbon shift.

EP4 provides the counterexample. It has $\Delta^{13}CH_3D$ of 1.58 ‰, close to heated EP6, but its $\Delta^{12}CH_2D_2$ value reaches 17.34 ‰ and its δD–CH_4 value is only -39.93 ‰. This combination is not a continuation of thermal contraction; it is a hydrogen-rich dual-clump departure. EP4 would be misclassified if only $\Delta^{13}CH_3D$ were considered.

The δD–CH_4–$\Delta^{12}CH_2D_2$ contrast is shown in Figure 11. This plot emphasizes the association between hydrogen-rich bulk composition and extreme $\Delta^{12}CH_2D_2$ enrichment.

The separation displayed in Figure 11 strengthens the EP4 assignment. The gas is not merely high in one clumped coordinate; it combines very high $\Delta^{12}CH_2D_2$ with a much less negative δD–CH_4 value than the other EP gases. The paired bulk-and-clumped behavior supports a

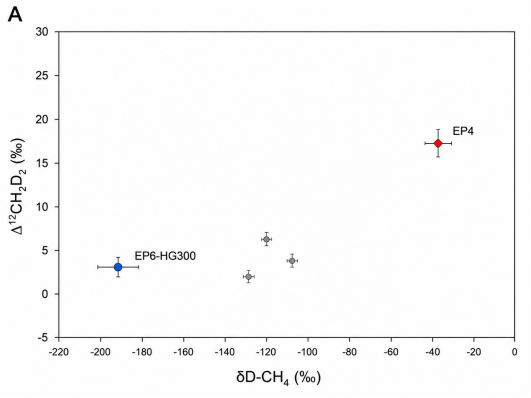

Figure 11: Hydrogen-rich $\Delta^{12}CH_2D_2$ departure.

hydrogen-rich departure rather than a low-clump thermal endpoint. The paired clumped-coordinate comparison is presented in Figure 12. The plot tests whether EP4 and EP6-HG300 remain separated when only the two mass-18 coordinates are considered.

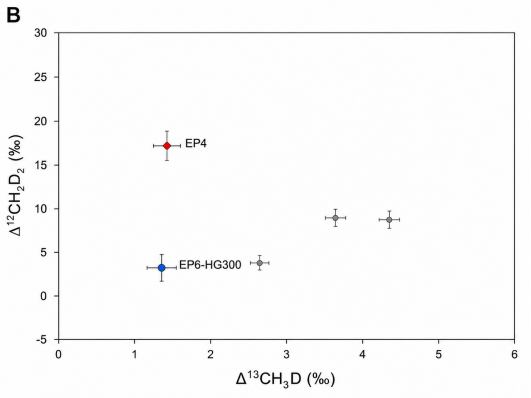

Figure 12: Paired clumped-coordinate separation.

The paired plot in Figure 12 answers a central part of the research question. EP4 and EP6-HG300 lie close in $\Delta^{13}CH_3D$ but far apart in $\Delta^{12}CH_2D_2$. A single-coordinate reading would merge two chemically different states, whereas the paired coordinate space preserves their difference. This distinction agrees with evidence that kinetic, exchange, and microbial processes can move methane through $\Delta^{13}CH_3D$–$\Delta^{12}CH_2D_2$ space along paths unlike pure thermal equilibration [11, 15, 17, 18].

3.4. Dual-clump reference space and gas classes

The class-separation indices are summarized in Table 5. EP6 has zero displacement because it is used as the reference coordinate. EP1 remains close to EP6, EP7 shifts toward a lower-clump field, EP6-HG300 occupies a heated low-clump field, and EP4 has a disproportionate $\Delta^{12}CH_2D_2$-to-$\Delta^{13}CH_3D$ proportion of 10.97.

Table 5: Class-separation indices.

Gas	$\Delta^{12}CH_2D_2$ relative to $\Delta^{13}CH_3D$	Displacement from EP6	Gas class
EP6	2.47	0.00‰	High-clump reference coordinate
EP1	2.12	0.54‰	Near-reference high-clump gas
EP7	1.47	5.18‰	Low-clump displaced gas
EP6-HG300	1.93	5.95‰	Heated low-clump gas
EP4	10.97	8.74‰	Hydrogen-rich dual-clump departure

The indices in Table 5 show that coordinate distance and coordinate proportion carry different information. EP6-HG300 and EP7 have comparable displacement magnitudes from EP6, but the heated gas is more diagnostic of molecular reordering because its bulk carbon isotope composition stays close to EP6. EP4 has the largest displacement and an extreme coordinate proportion, making it a separate gas class rather than an endpoint of the high-clump to low-clump sequence.

The final reference space is displayed in Figure 13. The regions represent calibration classes defined by the EP-gas relationships rather than statistical clusters from a large population.

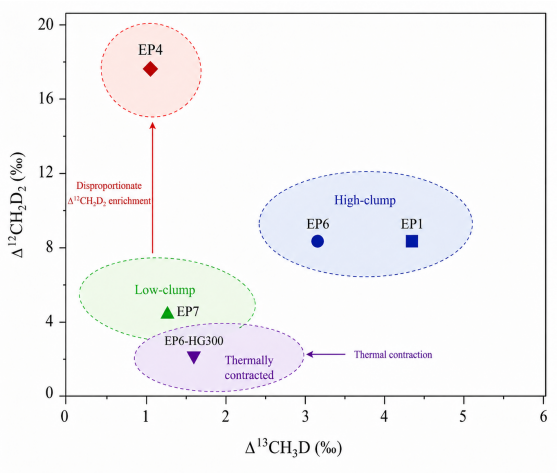

Figure 13: Dual-clump reference space.

The reference space in Figure 13 provides the main classification result. EP6 and EP1 form the high-clump reference region; EP7 moves downward in both clumped coordinates; EP6-HG300 marks thermal contraction with preserved bulk-carbon similarity; and EP4 forms a hydrogen-rich departure. The classification comes from paired-coordinate geometry combined with spectral leverage, not from an undifferentiated isotope-field label.

3.5. Interlaboratory transfer and broader analytical context

Interlaboratory behavior is essential for calibration transfer. EP6 spans 3.11–3.65‰ in $\Delta^{13}CH_3D$ and 7.19–8.90‰ in $\Delta^{12}CH_2D_2$. EP1 spans 3.92–4.10‰ in $\Delta^{13}CH_3D$ and 8.63–9.43‰ in $\Delta^{12}CH_2D_2$. EP7 spans 2.31–2.78‰ in $\Delta^{13}CH_3D$ and 3.09–3.76‰ in $\Delta^{12}CH_2D_2$. These ranges do not invalidate the reference gases; they show why laboratory spread must remain visible alongside representative coordinates.

A leverage-normalized reference space makes two uncertainty sources visible at the same time. Spectroscopic uncertainty comes from the local line environment, especially the weak $^{12}CH_2D_2$ line. Calibration-transfer uncertainty comes from laboratory differences in measured gas coordinates. A classification is strongest when both uncertainty sources still support the same gas assignment. EP4 meets that condition because its $\Delta^{12}CH_2D_2$ enrichment greatly exceeds the observed reference-gas spread. EP6-HG300 also meets it because both clumped coordinates decrease strongly relative to EP6 while bulk carbon remains nearly unchanged.

The broader natural-gas context is shown in Figure 14. This comparison connects the EP-gas classes with methane clumped-isotope literature without converting the calibration exercise into a natural-sample survey.

The contextual view in Figure 14 reinforces the need for paired interpretation. Bulk isotope fields can overlap, and natural methane can depart from equilibrium through microbial, thermogenic, abiotic, or alteration processes [16, 20, 23]. The EP gases analyzed here do not span the entire natural range. Their value is that they define controlled analytical contrasts for testing whether an instrument and calibration protocol preserve the distinction between heated low-clump methane and hydrogen-rich departure.

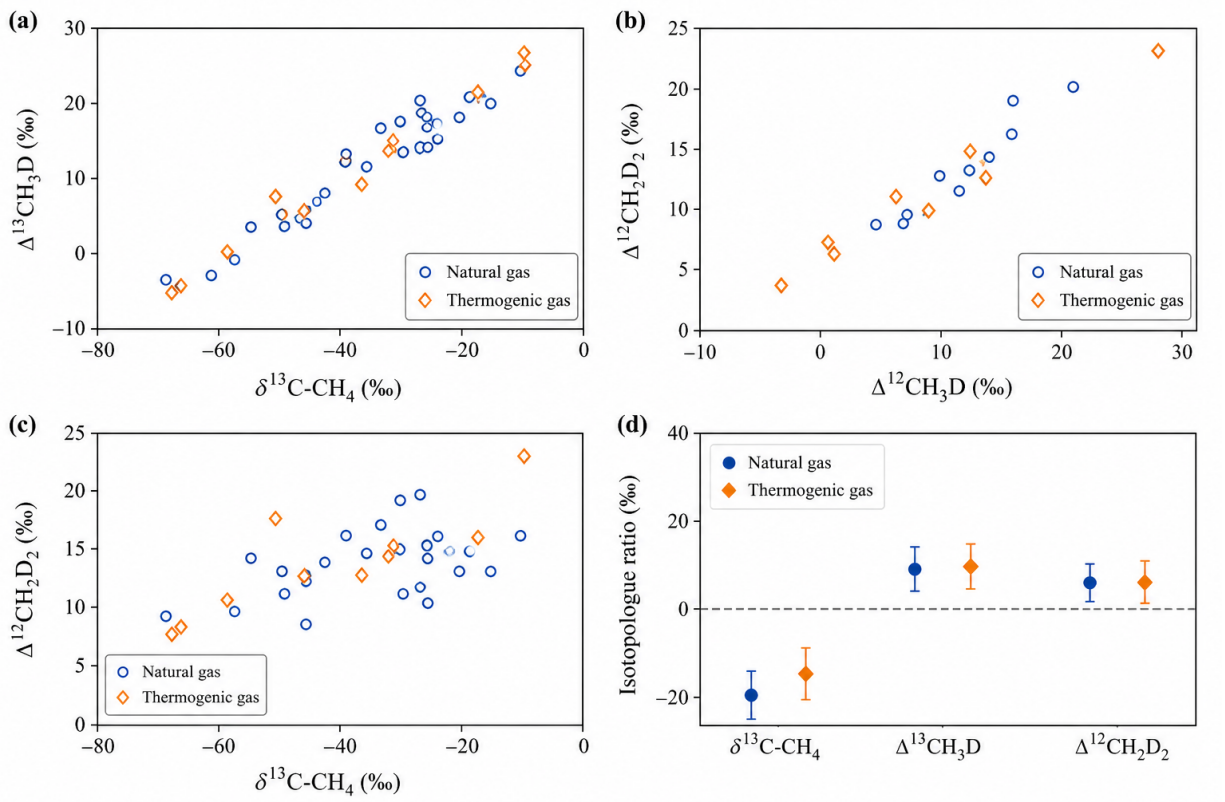

Figure 14: Natural and thermogenic context.

The analytical contribution has two parts. First, local spectral leverage must accompany clumped-isotope interpretation when mid-infrared absorption windows are used. Second, a small EP-gas set can support meaningful classification when the gases represent high-clump, low-clump, heated, and hydrogen-rich states. These findings are directly relevant to analytical spectroscopy and instrumentation because they link line selection, measurement confidence, and calibration transfer to chemical interpretation.

3.6. Analytical constraints and validation requirements

The calculation is based on tabulated line and isotope values. It does not replace full spectral retrieval, pressure-series fitting, detector-noise characterization, residual analysis, gas-purity checks, or covariance modeling. Line-strength share is a compact measure of local leverage, not a complete error model. Similarly, uncertainty-weighted consolidation cannot eliminate systematic laboratory offsets, especially when laboratories use different instruments, inlet systems, fitting procedures, or reference scales.

Validation of the same calibration logic requires retrieval diagnostics to be reported with the final $\Delta^{13}CH_3D$ and $\Delta^{12}CH_2D_2$ values. Residual structure in the two laser windows, pressure-dependent tests of the weak $^{12}CH_2D_2$ transition, and repeated measurements of identical gas aliquots would determine how much of the observed spread arises from spectroscopy rather than gas preparation or reference-scale transfer. Additional reference gases between EP6-HG300 and EP4 would test whether hydrogen exchange produces gradual movement in δD–CH_4–$\Delta^{12}CH_2D_2$ space or an abrupt endpoint-like departure.

4. Conclusions

The results answer the research question by showing that a leverage-normalized EP-gas reference space can separate thermally heated methane from hydrogen-rich and low-clump methane states, but only when $\Delta^{13}CH_3D$ and $\Delta^{12}CH_2D_2$ are interpreted as unequal measurement coordinates. The $^{12}CH_2D_2$ transition represents 1.10% of the laser-1 line-strength total, whereas $^{13}CH_3D$ represents 11.29% of the laser-2 total. This difference means that $\Delta^{12}CH_2D_2$ carries exceptional diagnostic value but must be read as a line-limited coordinate, while $\Delta^{13}CH_3D$ has stronger direct leverage but remains affected by neighboring major-isotopologue absorptions.

The reference gases form four distinct analytical classes. EP6 and EP1 are high-clump gases, with representative $\Delta^{13}CH_3D/\Delta^{12}CH_2D_2$ coordinates of 3.58/8.83 ‰ and 4.10/8.67 ‰, respectively. EP7 is a lower-clump displaced gas because both clumped coordinates decrease relative to EP6 while bulk isotope composition also shifts. EP6-HG300 defines the heated class: $\Delta^{13}CH_3D$ decreases from 3.58 ‰ to 1.66 ‰ and $\Delta^{12}CH_2D_2$ decreases from 8.83 ‰ to 3.20 ‰ while the Empa $\delta^{13}C$–CH_4 coordinate remains essentially unchanged. EP4 defines the hydrogen-rich class: its $\Delta^{13}CH_3D$ value of 1.58 ‰ resembles heated EP6, but its $\Delta^{12}CH_2D_2$ value of 17.34 ‰ and much less negative δD–CH_4 value place it outside the heated low-clump trajectory.

The specific conclusion is that calibration for mid-infrared methane clumped-isotope spectroscopy must preserve both dimensions of the paired mass-18 coordinate system and must report the line-strength environment supporting each coordinate. A one-axis interpretation would risk grouping EP4 with heated methane, whereas the paired $\Delta^{13}CH_3D$–$\Delta^{12}CH_2D_2$ reference space separates high-clump, low-clump, heated, and hydrogen-rich methane states. The conclusion is therefore analytical rather than rhetorical: gas classification depends on measurement selectivity, reference-gas transfer, and spectroscopy-aware uncertainty.

References

[1] Whiticar, M. J. (1999). Carbon and hydrogen isotope systematics of bacterial formation and oxidation of methane. *Chemical Geology*, *161*(1–3), 291–314.

[2] Stolper, D. A., Lawson, M., Davis, C. L., Ferreira, A. A., Neto, E. S., Ellis,

G. S., ... & Eiler, J. M. (2014). Formation temperatures of thermogenic and biogenic methane. *Science*, *344*(6191), 1500–1503.
[3] Stolper, D. A., Martini, A. M., Clog, M., Douglas, P. M., Shusta, S. S., Valentine, D. L., ... & Eiler, J. M. (2015). Distinguishing and understanding thermogenic and biogenic sources of methane using multiply substituted isotopologues. *Geochimica et Cosmochimica Acta*, *161*, 219–247.
[4] Douglas, P. M., Stolper, D. A., Eiler, J. M., Sessions, A. L., Lawson, M., Shuai, Y., ... & Kitchen, N. (2017). Methane clumped isotopes: Progress and potential for a new isotopic tracer. *Organic Geochemistry*, *113*, 262–282.
[5] Ghosh, P., Adkins, J., Affek, H., Balta, B., Guo, W., Schauble, E. A., ... & Eiler, J. M. (2006). $(^{13}C) - -(^{18}O)$ bonds in carbonate minerals: A new kind of paleothermometer. *Geochimica et Cosmochimica Acta*, *70*(6), 1439–1456.
[6] Wang, Z., Schauble, E. A., & Eiler, J. M. (2004). Equilibrium thermodynamics of multiply substituted isotopologues of molecular gases. *Geochimica et Cosmochimica Acta*, *68*(23), 4779–4797.
[7] Eiler, J. M. (2007). "Clumped-isotope" geochemistry—The study of naturally occurring, multiply substituted isotopologues. *Earth and Planetary Science Letters*, *262*(3–4), 309–327.
[8] Eldridge, D. L., Korol, R., Lloyd, M. K., Turner, A. C., Webb, M. A., Miller, T. F., III, & Stolper, D. A. (2019). Comparison of experimental vs theoretical abundances of $(^{13}CH_3D)$ and $(^{12}CH_2D_2)$ for isotopically equilibrated systems from 1 to 500 (°C). *ACS Earth and Space Chemistry*, *3*(12), 2747–2764.
[9] Ono, S., Wang, D. T., Gruen, D. S., Sherwood Lollar, B., Zahniser, M. S., McManus, B. J., & Nelson, D. D. (2014). Measurement of a doubly substituted methane isotopologue, $(^{13}CH_3D)$, by tunable infrared laser direct absorption spectroscopy. *Analytical Chemistry*, *86*(13), 6487–6494.
[10] Stolper, D. A., Sessions, A. L., Ferreira, A. A., Neto, E. S., Schimmelmann, A., Shusta, S. S., ... & Eiler, J. M. (2014). Combined (^{13}C)–D and D–D clumping in methane: Methods and preliminary results. *Geochimica et Cosmochimica Acta*, *126*, 169–191.
[11] Young, E. D., Kohl, I. E., Lollar, B. S., Etiope, G., Rumble, D., III, Li, S., ... & Bryndzia, L. T. (2017). The relative abundances of resolved $(^{12}CH_2D_2)$ and $(^{13}CH_3D)$ and mechanisms controlling isotopic bond ordering in abiotic and biotic methane gases. *Geochimica et Cosmochimica Acta*, *203*, 235–264.
[12] Wang, X., Liu, C. Q., Zhang, N., Xu, S., Pang, Z., Li, S. L., ... & Ellam, R. M. (2023). Clumped methane isotopologues $((^{13}CH_3D)$ and $(^{12}CH_2D_2))$ of natural samples measured using a high-resolution mass spectrometer with an improved pretreatment system. *Journal of Analytical Atomic Spectrometry*, *38*(1), 186–196.
[13] Gonzalez, Y., Nelson, D. D., Shorter, J. H., McManus, J. B., Dyroff, C., Formolo, M., ... & Ono, S. (2019). Precise measurements of $(^{12}CH_2D_2)$ by tunable infrared laser direct absorption spectroscopy. *Analytical Chemistry*, *91*(23), 14967–14974.
[14] Zhang, N., Prokhorov, I., Kueter, N., Li, G., Tuzson, B., Magyar, P. M., ... & Mohn, J. (2025). Rapid high-sensitivity analysis of methane clumped isotopes $((\Delta^{13}CH_3D)$ and $(\Delta^{12}CH_2D_2))$ using mid-infrared laser spectroscopy. *Analytical Chemistry*, *97*(2), 1291–1299.
[15] Wang, D. T., Gruen, D. S., Lollar, B. S., Hinrichs, K. U., Stewart, L. C., Holden, J. F., ... & Ono, S. (2015). Nonequilibrium clumped isotope signals in microbial methane. *Science*, *348*(6233), 428–431.
[16] Shuai, Y., Etiope, G., Zhang, S., Douglas, P. M., Huang, L., & Eiler, J. M. (2018). Methane clumped isotopes in the Songliao Basin (China): New insights into abiotic vs. biotic hydrocarbon formation. *Earth and Planetary Science Letters*, *482*, 213–221.
[17] Ono, S., Rhim, J. H., Gruen, D. S., Taubner, H., Kölling, M., & Wegener, G. (2021). Clumped isotopologue fractionation by microbial cultures performing the anaerobic oxidation of methane. *Geochimica et Cosmochimica Acta*, *293*, 70–85.
[18] Liu, J., Harris, R. L., Ash, J. L., Ferry, J. G., Krause, S. J., Labidi, J., ... & Young, E. D. (2023). Reversibility controls on extreme methane clumped isotope signatures from anaerobic oxidation of methane. *Geochimica et Cosmochimica Acta*, *348*, 165–186.
[19] Liu, J., Treude, T., Abbasov, O. R., Baloglanov, E. E., Aliyev, A. A., Harris, C. M., ... & Young, E. D. (2024). Clumped isotope evidence for microbial alteration of thermogenic methane in terrestrial mud volcanoes. *Geology*, *52*(1), 22–26.
[20] Defratyka, S. M., Fernandez, J. M., Adnew, G. A., Dong, G., Douglas, P. M., Eldridge, D. L., ... & Arnold, T. (2025). Global inventory of doubly substituted isotopologues of methane $((\Delta^{13}CH_3D)$ and $(\Delta^{12}CH_2D_2))$. *Earth System Science Data Discussions*, *2025*, 1–30.
[21] Rothman, L. S., Gordon, I. E., Babikov, Y., Barbe, A., Benner, D. C., Bernath, P. F., ... & Wagner, A. G. (2013). The HITRAN2012 molecular spectroscopic database. *Journal of Quantitative Spectroscopy and Radiative Transfer*, *130*, 4–50.
[22] Gordon, I. E., Rothman, L. S., Hargreaves, E. R., Hashemi, R., Karlovets, E. V., Skinner, F. M., ... & Yurchenko, S. N. (2022). The HITRAN2020 molecular spectroscopic database. *Journal of Quantitative Spectroscopy and Radiative Transfer*, *277*, 107949.
[23] Wang, D. T., Reeves, E. P., McDermott, J. M., Seewald, J. S., & Ono, S. (2018). Clumped isotopologue constraints on the origin of methane at seafloor hot springs. *Geochimica et Cosmochimica Acta*, *223*, 141–158.